Hindawi Publishing Corporation
Journal of Sensors
Volume 2016, Article ID 7235984, 14 pages
http://dx.doi.org/10.1155/2016/7235984

Research Article

Autonomous WiFi Sensor for Heating Systems in the Internet of Things

C. A. Trasviña-Moreno, R. Blasco, R. Casas, and A. Marco

Instituto de Investigación en Ingeniería de Aragón, Universidad de Zaragoza, 50018 Zaragoza, Spain

Correspondence should be addressed to C. A. Trasviña-Moreno; trasvina@unizar.es

Received 30 September 2015; Revised 10 December 2015; Accepted 16 December 2015

Academic Editor: Vincenzo Paciello

In smart cities and home applications, the use of Wireless Sensor Networks to extract environmental data becomes more common with the passing of time. These sensors are used for a wide array of applications, but mainly to manage energy consumption in domestic buildings. One of the key energy consumers in households is heating systems. To monitor them, sensors are used with wireless communication protocols, like ZigBee, to transmit data to a central processing unit (CPU). WiFi communications, on the contrary, are rarely seen in these implementations due to its high energy consumption, although almost in every home one can find such networks. Yet, with the Internet of Things (IoT), new revisions of the standard have arisen which enable this technology for wireless sensing. To validate this theory and fill a technological necessity, this proposal is presented. In this work, the design and implementation of an autonomous WiFi sensor, paired with thermoelectric energy harvesting, are presented as an IoT solution for monitoring heating devices. For this, a thorough analysis of the proposed architecture is presented. Tests regarding energy consumption and generation, efficiency, and real world scenario trials are done. Finalizing, a comparison between the obtained results and current implementations is shown.

1. Introduction

In current times, there is a great interest in having control over energy consumption in home environments. This generates a large market demand for devices that monitor such variables indoor. Currently, this is covered by Wireless Sensor Networks (WSN) which can be widely varied in their architecture, using different means for communication, energy management and storage, sensor devices, and so forth. Depending on the variable or device that is to be monitored, these may also vary greatly.

One of the most power demanding systems in these indoor scenarios is the heating systems, which usually are comprised of several heat radiators distributed along the different spaces of a household.

In Spain, there are over one million households that have centralized heating (CH) systems [1]. According to a study made in Italy, where these type of systems are also common, they present a low energy efficiency compared to that of independent units [2]. Due to the nature of CH systems, the amount of energy used by each dwelling habitat is normally divided equally amongst all tenants. This type of energy management creates uneven situations, as some users may not use the heating system on a regular basis, while others will exceed its usage; yet, all will be charged the same fair. Thus, the cost of usage for these systems is divided without taking in account the individual consumption of each habitat.

These type of CH systems which lack effective control and monitoring mechanisms, as well as behavioural patterns of the less conscious house dwellers [3], generate an environment where there is little interest in energy efficiency and energy-saving measures.

According to the 2012/27/UE directive of the European Parliament and the Energy Efficiency Council, in its 9th article [4], it will be required that all end users of these type of heating systems install an individual energy counter which will reflect its actual energy consumption. Moreover, it will provide the users with real-time, or near real-time, data regarding its usage. This directive states that, in Europe,

all households should have these type of "energy auditors" before the 31st of December of 2016. This applies to all households, with either individual or centralized heating systems.

Due to this, and similar requirements, in home automation and smart buildings, it is common to find smart devices in constant communication. According to their communication range, they can be classified in short- and mid-range communication devices. In short-range communications, it is common to find protocols such as Bluetooth, ultrawide band, and infrared data association, whilst in mid-range communications, the most common are 802.15.4 based protocols [5], such as ZigBee, and 802.11 protocols [6], like WiFi [7]. It is common to find applications and proposals for sensor devices that utilize ZigBee communications, as it is one of the most energy efficient protocols available [8, 9]. Yet, this protocol has a major drawback that it requires a dedicated network deployment which is uncommon in home environments. On the other hand, WiFi is probably one of the most well-known and sought out protocols in the market [10–12]. Its network deployments can be found almost in every household and even in other types of urban scenarios. However, the original design of WiFi was not thought of for low power devices or low data rates. In current times, with the coming of Internet of Things (IoT), this protocol has gone thru new revisions which allow low power modes and other benefits, making it more suitable for low power smart devices.

With the recent changes that WiFi presents, it has opened doors to new possibilities for powering smart low power WiFi devices. One of the most interesting ones is energy harvesting. This type of technology takes advantage of ambient sources, such as light emissions, thermal variations, and radio frequency, and converts them into electrical energy [13, 14]. These type of environmental sources can also be found and put to good use, in urban buildings and households [15]. Depending on the selected energy source to harvest, different techniques, as well as electronic devices, must be used to extract the most amount of energy possible in an efficient manner. The use of energy harvesting in smart sensors and devices enables the possibility of discarding standard batteries, which present a limited life span. By consequence, the use of batteries limits the use of the smart devices and forces the user to constantly replace these if he wishes to continue utilizing the device. With the use of energy harvesting techniques, as well as low power electronics, it is possible to increase the life expectancy of a smart device to an almost unlimited amount.

In this paper, an analysis of viability, design, and real world test of a WiFi sensor with energy harvesting for home radiators was realized. Compared to other implementations, the key differentiator in this work is the use of WiFi communications. Utilizing WiFi, compared to other protocols, simplifies the implementation of WSN as the infrastructure is already laid in the majority of households and buildings. Also, it provides a direct link to the cloud, while other technologies would require a bridge device with Ethernet or WiFi communications. This will provide an easy solution to adapt CH and outdated systems, to the newly established directive at a reasonable cost. Additionally, this device may be used to capture other environmental data, using the same architecture, which could provide a more global and controlled perspective of its surroundings. To accomplish this, first, a comprehensive study of implementations related to sensor devices for heating systems in households was done, and the most relevant are described in the following section. Afterwards, the architecture of this proposal is explained in detail, subdividing it in its key sections. Then, tests and their results, as well as a discussion of the outcome, are shown. To finalize, possible future work lines and the conclusions, according to the stated objectives, are presented.

2. Related Work

In smart home environments, several studies have been made on WSN, some focusing more on the communication protocol and others on energy autonomy.

Wang et al. [16] present a similar approach for energy management to the one proposed in this paper. For their proposal, they had a custom built thermoelectric generator, as well as a three-stage energy harvesting conversion module to provide energy to their sensor device, or mote. With it, they have proved to achieve a global energy efficiency of 25.2%. This specific mote presented ZigBee wireless communications.

Han et al. [17] propose a home energy monitoring system which utilizes ZigBee as communications protocol to transmit consumption data to a central server for analysis. This data, in conjunction with others provided by PLC communications, is used to provide information to the user and allow for a personal management of the energy from a UI.

Kelly et al. [18] describe a home energy monitoring system focused on IoT technologies. By utilizing ZigBee to communicate amongst the sensor nodes and an IPV6 gateway that translates to UDP packets and sends the information to the internet, they monitor parameters such as temperature, humidity, and light, to assess the home energy consumption.

Nguyen and Le-trung [19] propose a low power battery charged WiFi solution for motes in smart building. Their main focus is on optimizing the hardware and software architecture of the mote, achieving a lifetime of 46 days with four 3.7 V 4200 mAh batteries.

These are just some examples of current applications, but as seen in the previously mentioned work, the majority of implementations utilize ZigBee communications. The ZigBee protocol is presented as one of the most widely used in WSN due to its low power characteristics. To integrate sensors with cloud computing and IoT, other authors have opted for ZigBee hybrid network connected to a WiFi or Ethernet gateway [20], similar to the work presented by Kelly et al. [18]. Few proposals utilize solely WiFi communications in smart home environments, and the majority of them power these devices with standard batteries or connected to the main power grid. These reasons are presented as the principal motivation of this work, as well as the study of other viable alternatives which simplify the interaction of users with IoT in home environments.

In the following section, the hardware and firmware design of this proposal will be analysed. This will allow

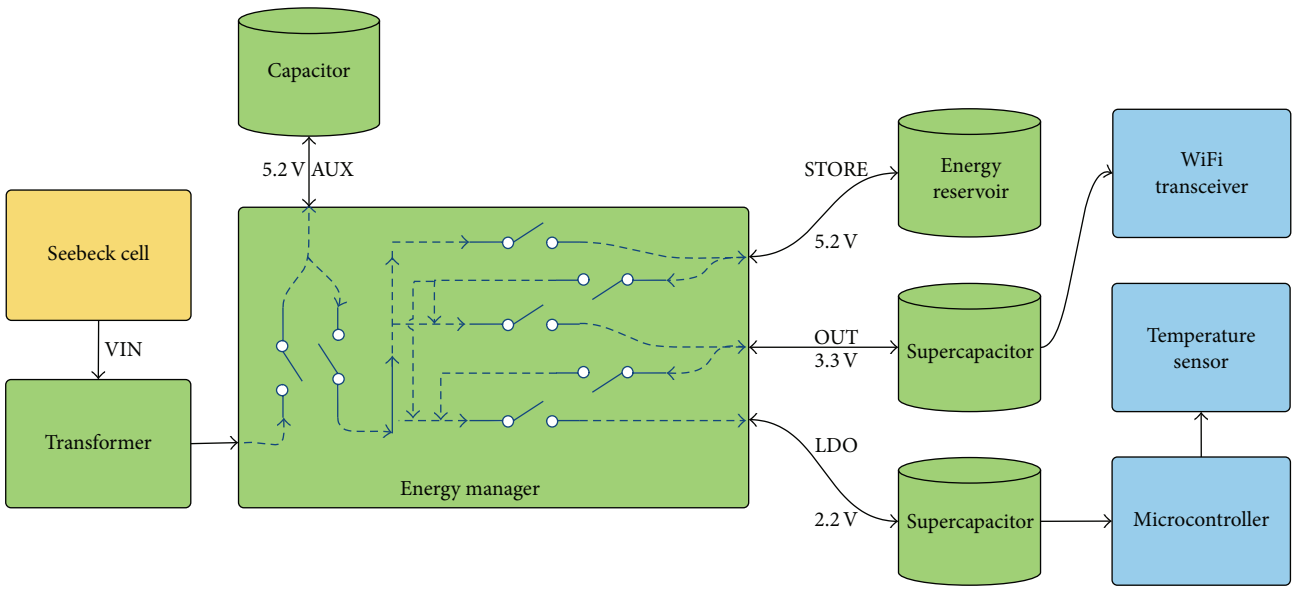

Figure 1: Block diagram of the mote, its energy distribution, and the internal energy flow for the energy manager IC.

the reader to better understand some of the requirements needed if a similar work were to be realized.

3. Proposed Architecture

As previously mentioned, the proposed architecture will differ from current implementations by utilizing solely WiFi communications protocol, and by being complimented by a thermal energy harvester as its power source (Figure 1).

In Figure 1, it is possible to view an abstract representation of the functionality and energy distribution of the energy management IC. This device is represented as an "energy multiplexor," providing energy to its different outputs as needed. Further details on its functionality will be described in Section 3.4.

In this section, the following subjects will be addressed, so as to clearly depict the different areas that were involved in the architecture design:

(i) Selected hardware and improvements.

(ii) Low power firmware implementation.

(iii) Ambient energy transducer.

(iv) Ambient energy conversion and management.

3.1. Hardware. In order to promote the use of open source hardware, the proposed sensor node was based on an open architecture, namely, the Flyport WiFi module [21]. This unit is comprised mainly of a PIC24FJ256GA106 microcontroller (MCU) [22] and a MRF24WB0MA WiFi module [23], which serve as a central processing unit and wireless communications, respectively. These present low power characteristics and modes which, although not cutting edge, will serve as a baseline for future work.

To improve the characteristics of the Flyport, the original hardware design was modified to reduce the overall consumption of the board. Unnecessary elements such as LEDs, external LDO, and diodes were removed. The main power line was split in two, one for the MCU at 2.2 V and another for the transceiver at 3.3 V. Lastly, a voltage level translator was added for the SPI communications between the MCU and transceiver.

Given that at low voltage levels both the MCU and transceiver start to increase their current consumption, which impacts directly the start-up of the load, switch type circuits were also implemented for both these devices. For the MCU, a SET/RESET circuit was added, which is enabled by a pin from the energy management IC, called PGD, and may be disabled by the MCU. The PGD pin is a digital output that is set to high (2 V) when the OUT output reaches 92.5% of its nominal value. The transceiver, on the other hand, has a MOSFET switch circuit which is enabled by a MCU signal on-demand.

3.2. Firmware. Firmware modifications were done keeping in mind low power strategies as the main orientation (Figure 2). For the initial start-up of the MCU, the 31 kHz internal RC oscillator (LPRC) was used, which reduces the boot-up consumption. Also, all unused peripherals, such as timers, UARTS, and secondary SPI modules, were disabled. The ADC peripheral is enabled only when the sensor needs to be activated; afterwards, it is disabled and its voltage reference is set to GND. Also, the temperature sensor is activated by a digital I/O of the MCU, which is also enabled and disabled with the ADC. Once it is time to transmit, in its first iteration, the oscillator is switched to the high speed 32 MHz clock source and the RTOS, which mostly manages the WiFi activities, is initialized. Finally, both the MCU and transceiver, after finishing their corresponding activities, are set to the lowest

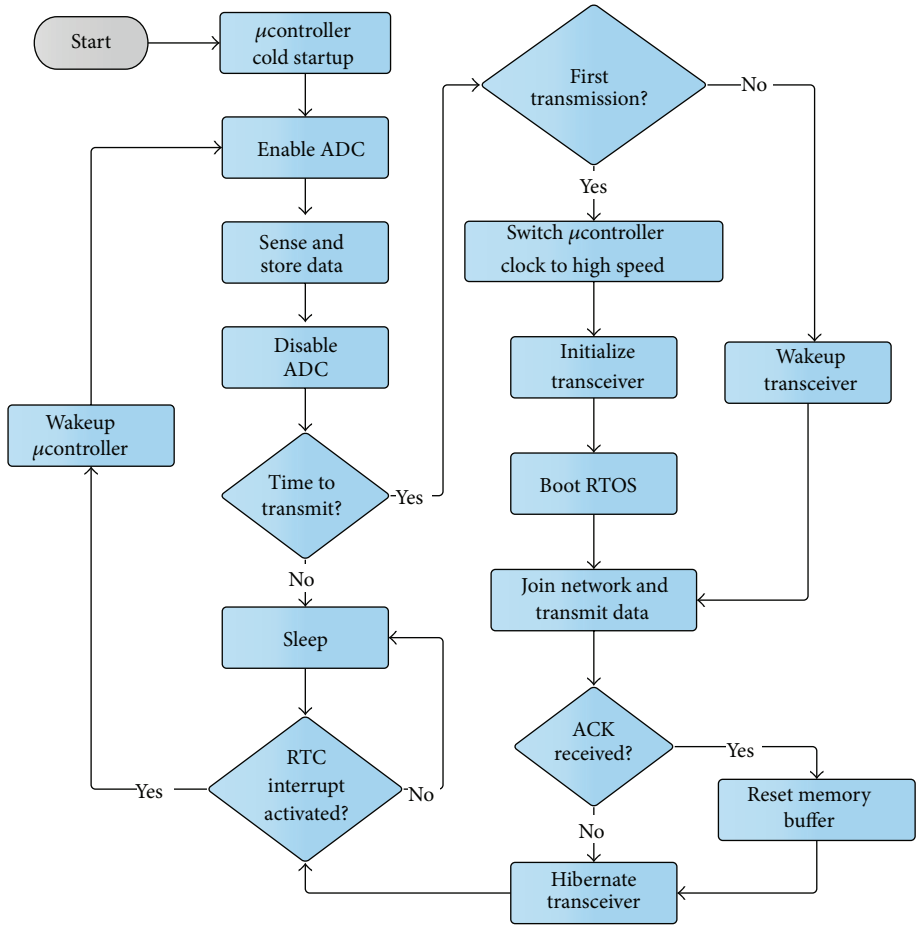

Figure 2: Workflow diagram of the WiFi sensor.

power mode available and are awoken by either the Real-Time Clock and Calendar (RTCC) alarm or internal flags.

3.3. Energy Source. The energy harvester (EH) module is comprised of a Peltier cell of 40×40×3.4 mm with an attached finned heat sink of 40×40×18 mm with no additional cooling mechanisms.

Although it is possible to increase the output of the Peltier cell with extra cooling, the desire of this study was to analyse the device in a nonoptimum and realistic environment, which would further validate more favourable scenarios (Figure 3).

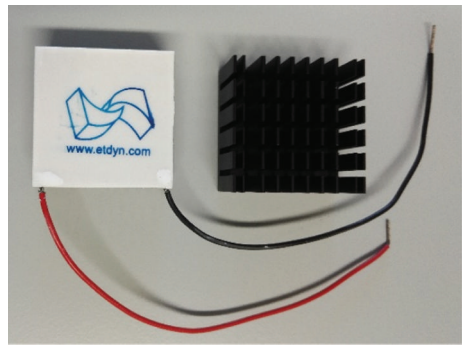

Figure 3: Seebeck cell with the finned heat sink.

3.4. Energy Management. To convert the captured ambient energy into more useful magnitudes, the LTC3108 [24] was selected as the core component. This IC will act as a step-up voltage converter and energy management system for the load and energy storage (Figure 1). This device has a static 2.2 V output (LDO), a configurable output (OUT) which was set at 3.3 V, and an additional output (STORE) to connect energy storage such as lithium batteries and supercapacitors. Internally, the LTC3108 distributes the energy similarly as a multiplexor would. An auxiliary capacitor acts as the main distributing line, which feeds the LDO, OUT, and STORE outputs, in that specific order. Once one of the outputs has reached its nominal voltage level, it continues to charge the next one (Figure 4).

When the circuit is loaded, the behaviour of the IC is less linear. If at any point the LDO output starts to demand more energy than the accumulated in the capacitor, it will draw energy from any available source (STORE, OUT, or AUX). Also, if the OUT output requires additional energy, it may draw only from the STORE or AUX sources. The main difference between these two is that the LDO output

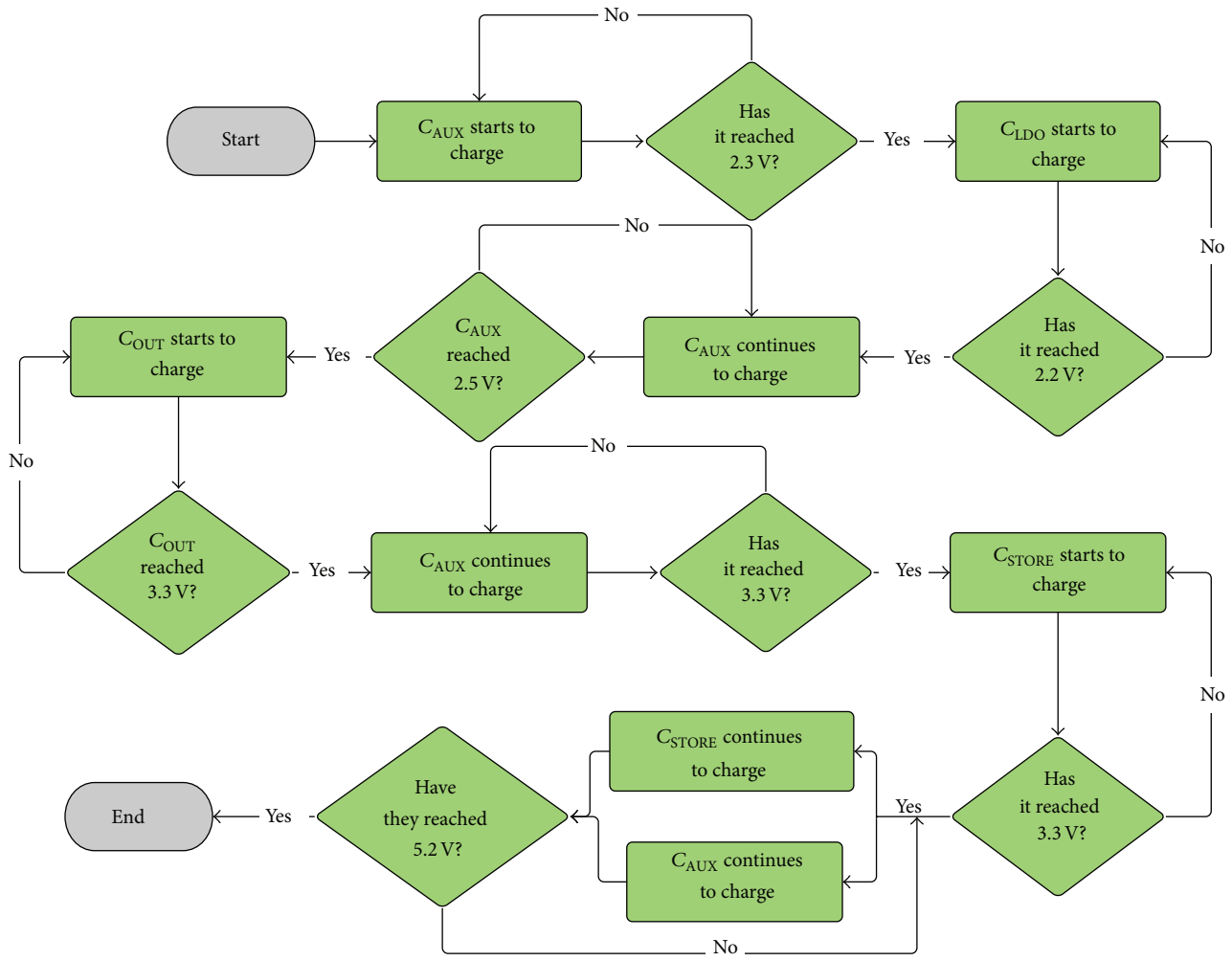

Figure 4: Energy manager charge workflow without load.

presents a higher priority than that of OUT and that the LDO will never lend energy to another output. It is important to note that the STORE output will only function in the case that there is additional energy. If all the energy generated is consumed by the load on LDO and OUT, then the STORE output may not be used.

Having described the architecture of this proposal, in the following section, the description of the theoretical and practical methods used to analyse the mote is given.

4. Tests and Results

In this section, a series of analyses and calculations are done for each block mentioned in the architecture. The main objectives are to

(i) understand the required energy for the load for a given time period,

(ii) understand the behaviour and capabilities of the thermoelectric generator (TEG),

(iii) validate the functionality and efficiency of the EH block,

(iv) confirm the functionality of the three blocks as a whole in a real world test environment.

To have a clear understanding of each block and the specific tests on each, this section is subdivided into (a) measuring equipment, (b) load energy characterization, (c) thermoelectric generator, (d) energy harvester, (e) mote validation, and (f) mote sustainability.

4.1. Measuring Equipment. To accomplish the previously mentioned goals, a series of tests and calculations were required. To acquire the needed data, such as voltage, current, and temperature, different laboratory equipment was used to measure the data with the highest precision available, including

(i) Tektronix MSO 2014 oscilloscope [25],

(ii) Tektronix DMM4050 digital multimeter [26],

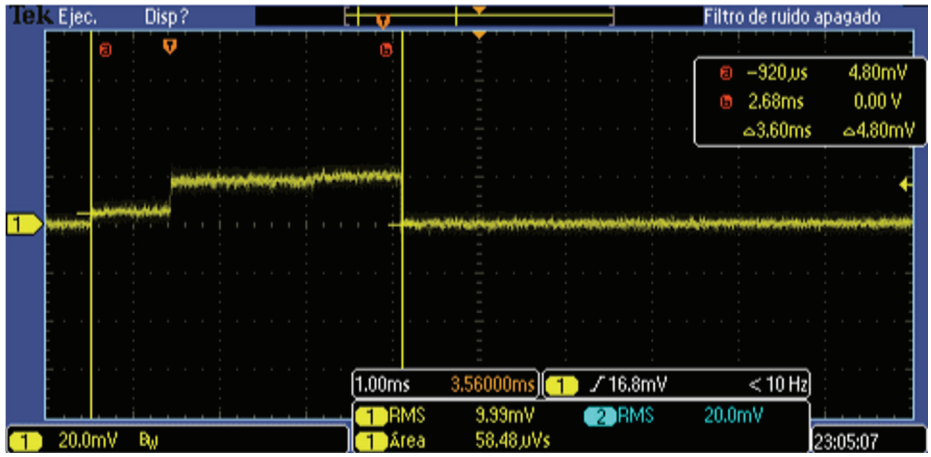

Figure 5: Charge consumed by the MCU while measuring temperature. Vertical scale at 20 mV/div and horizontal scale at 1 ms/div.

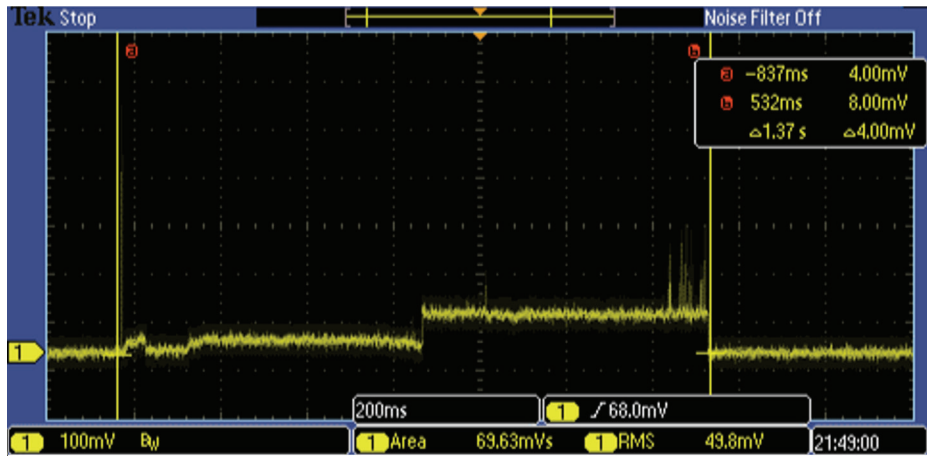

Figure 6: Charge consumed by the transceiver while transmitting data. The signal level was lowered below zero to avoid losing charge spikes and alter the measured value. Vertical scale at 100 mV/div and horizontal scale at 200 ms/div.

(iii) Pico Technology TC-08 thermocouple data logger [27],

(iv) Type-K thermocouples,

(v) National Instruments LabView [28].

4.2. Load Energy Characterization. The load is comprised mainly of a MCU, a WiFi transceiver, and a temperature sensor. In prior studies [29], a theoretical analysis of these devices was made with the purpose of understanding their consumption levels. From this analysis, the MCU and transceiver were identified as the primary consumers of the load, and the energy consumption of the sensor can be considered, in most cases, as negligible. To understand the actual energy needs of these two devices, measurements were required to be done of their active and inactive states individually. For this task, the previously mentioned measuring equipment was connected to a PC thru a serial port, using a LabView-based interface, to capture all the data for posterior analysis. It is important to note that all the transmissions were made using the TCP internet protocol, mainly for security and data continuity reasons.

To measure the active stages, the area under the curve was extracted with the oscilloscope and a 1 Ω shunt resistor placed on the high-side of each device (Figures 5 and 6).

For the active transmitting state of the microcontroller, the charge consumed by the device is not displayed given that it has a linear consumption with the same period of time as Figure 6. For each active state, several measurements were made from which the average charge was extracted. Given that a 1 Ω resistor was used to extract these values and the area under the curve is given in voltage per second, a direct extraction of the charge value can be done. For the inactive power stages, the current was measured with the digital multimeter and the average value was also calculated. Lastly, all the extracted data was converted to energy, providing a single comparable unit of measure amongst the devices (Table 1).

In Table 1, three key states and their consumption are displayed. To perform a sensor measurement, the only required device is the MCU; thus, the transceiver is not accounted for

Table 1: Average energy consumption of the main devices of the load in their active and inactive states.

State	MCU	Transceiver
Sensing	146.3 μJ	N/A
Transmitting	69.93 mJ	240.2 mJ
Inactive	24.2 μJ	1.65 μJ

in this activity. While transmitting data, both of the devices are required and are at their highest energy consumption levels. Lastly, during the inactive state, both devices display their lowest energy consumption.

To determine the energy consumption of the proposed sensor load, a similar approach is used as the one utilized in the theoretical analysis of a previous study [29]:

$$E_{\mathrm{CYCLE}} = E_{\mathrm{MC_{SENSE}}} + E_{\mathrm{MC_{TX}}} + E_{\mathrm{MC_{INACTIVE}}} + E_{\mathrm{RM_{TX}}} + E_{\mathrm{RM_{INACTIVE}}}. \quad (1)$$

Formula (1) shows the total energy per cycle calculations for the load. This formula does not include the start-up energy of the MCU or transceiver, as they are not repetitive on each cycle.

In this formula, E_{CYCLE} represents the total energy of the cycle, in joule, $E_{\mathrm{MC_{SENSE}}}$ is the MCUs energy consumed while sensing, $E_{\mathrm{MC_{TX}}}$ is the MCUs energy consumption in transmissions, $E_{\mathrm{MC_{INACTIVE}}}$ is the MCUs consumption while in low power, $E_{\mathrm{RM_{TX}}}$ is the transceivers consumed energy while transmitting, and $E_{\mathrm{RM_{INACTIVE}}}$ is the transceivers consumption while in low power mode.

To be able to calculate the energy of the cycle, an operating scenario must be selected. From a prior study [29], the most viable scenarios were chosen as starting point, where a transmission is done every hour and the amount of sensor measurements is varied. With the selected operation cycles, the predefined energy cycle formula, and the extracted measurements from the load, it was possible to extract the energy per cycle of each state for MCU and transceiver (Table 2).

As seen in Table 2, the energy drawn from the load is high compared to other implementations. The MCU itself is not from a low power device family, and it represents a large part of the consumed energy. One of the main drawbacks is its high sleep current, as in this state the device will be more than 90% of the time and it is noticeably higher than that of the transceiver. The WiFi transceiver presents a high active current consumption compared to other protocols but its total charge consumption is minimized by its low active periodicity as specified by the mote cycle.

Given these estimations, it is possible to understand the amount of energy that will be required from the energy harvesting stage for such an implementation. Thus, the next sections will describe the behaviour and energy expectations of the TEG, or Seebeck cell, and the energy harvesting module.

4.3. Thermoelectric Generator. To obtain energy from the heating device, a Seebeck cell was utilized as a transducer. Understanding the behaviour of the Seebeck cell is critical for the EH block, as it will help determine the best configuration for a maximum amount of energy extraction. For this purpose, measurements of voltage, current, and temperature difference, throughout a period of time, were made (Figure 7).

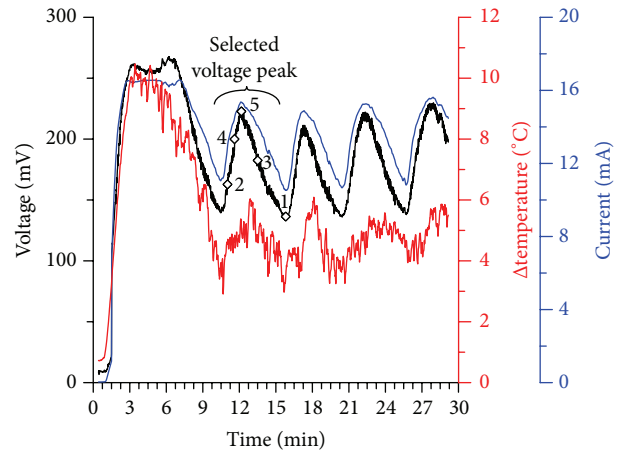

Figure 7: Seebeck cell performance test with voltage, current, and temperature difference measurements. Selected test points are depicted and numbered according to their increasing voltage value.

As can be seen in Figure 7, at the initial start-up, there is an increased energy generation due to the initialization of the heat radiator. Although useful for a faster start-up of the energy harvesting module, this peak cannot be considered for the estimation of the average conversion, as it represents a phase which will not occur frequently (e.g., each time the radiator is turned on). For the following measurements, the second peak in the graph was selected, as it represents a stable phase of energy conversion. From this peak, five voltage points were chosen, ranging from the lowest to the highest value, with their corresponding current value so as to calculate the power levels at each test point (Table 3).

Even though with the data shown in Figure 8 it is possible to extract the full range of power produced in the test peak, just a selection of these was thought to be a better representation, as they depict the clear operating variation of the Seebeck cell.

4.4. Energy Harvester. Once the TEG starts to generate energy, it is then transferred to the energy management IC for its conversion and management. For its proper functioning, this device requires an external transformer for the step-up conversion. The selection of the transformer is crucial to this IC as it will greatly affect the total efficiency of the energy harvesting, as mentioned by Wang et al. [16].

With the selected test points of Table 3 and the information provided in the datasheet of the energy management IC, at first glance, the 1 : 50 turn ratio transformer seems to be the best selection, as it maintains a more stable efficiency in the obtained voltage range. Yet, at these voltage levels, the current availability is low compared to the maximum tolerated, displayed in the datasheet. Additionally, the efficiency curves are drawn for output voltages of 4.5 V, instead of the 3.3 V configuration used in this proposal.

Table 2: Energy consumed by the load in each state.

One-hour cycle					
Measurements (per cycle)	Transmissions (per cycle)	MCU		Transmitter	
		Active energy (mJ)	Inactive energy (mJ)	Active energy (mJ)	Inactive energy (mJ)
360	1	122.5	87.1	240.2	5.9
60	1	78.6	87.1	240.2	5.9
6	1	70.7	87.1	240.2	5.9
1	1	70	87.1	240.2	5.9

Table 3: Test points of energy conversion from the selected voltage peak in Figure 8.

Test point	Voltage (mV)	Current (mA)	Power (mW)
1	137.24	10.67	1.46
2	160.55	12.85	2.06
3	185.94	14.03	2.60
4	207.02	14.78	3.06
5	224.10	15.35	3.44

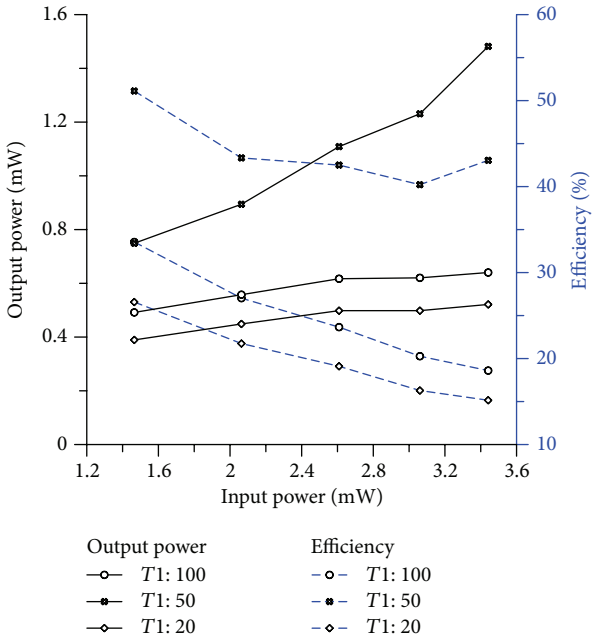

Figure 8: Transformer efficiency comparison of OUT at 3.3 V and the VIN input. The obtained power is shown with continuous lines and the efficiency with dashed lines.

To verify which turn ratio transformer was more favourable for the proposed scenario, a practical comparison between these was done by applying voltage and current from a configurable power source, emulating the TEG, for each test point described in Table 3. Voltage and current measurements were made at the main OUT, which led to the calculation of the power at these points, and afterwards the efficiency was extracted (Figure 8).

As seen in Figure 8, indeed, the 1 : 50 turn ratio presents itself as the best option for the current implementation.

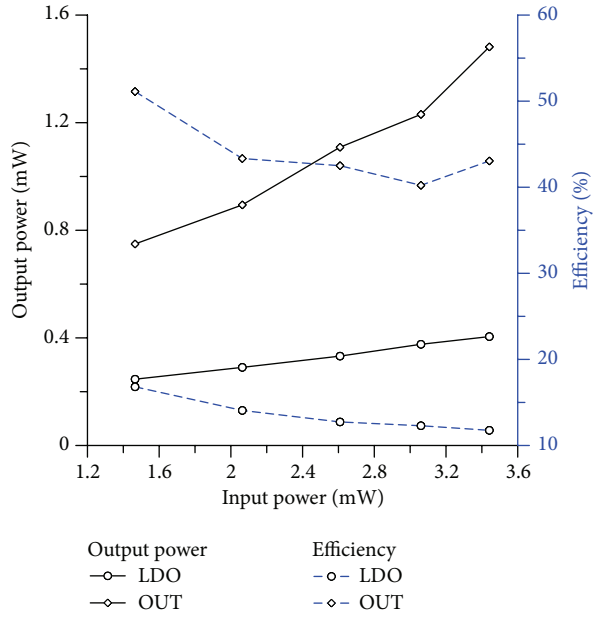

Figure 9: Power and efficiency comparison in charge regime. The obtained power is shown with continuous lines and the efficiency with dashed lines.

The main disadvantage of the utilization of this transformer is that, at the start-up, the initial voltage required by the harvester is higher than the 1 : 100 turn ratio. Although it is important to try to exploit every bit and scrap of energy, analysing the behaviour of the heat source, it is clear that the average amount of energy generated by the Seebeck cell will play a more key role in the long run.

Having selected the appropriate transformer for the energy harvesting module, with the same test points selected previously (Table 3), an analysis of power and efficiency for the LDO and OUT outputs is done. This data will help understand the limitations of the EH block, under the proposed scenario. It is important to understand that the energy management IC has two different work regimes, one for the initial charge of the LDO/OUT outputs and another for the case when the LDO/OUT outputs have reached their nominal values. From here on, these will be referred to as charge and stable regime accordingly. For both these analyses, it is assumed that there is no energy storage, as it will better depict a worst case scenario where energy is not sparing.

In Figure 9, it is possible to view the comparison of the LDO and OUT outputs in reference to the input provided by

Table 4: Energy harvesting block comparison with other relevant studies.

	Desai et al. [30]	Lhermet et al. [31]	Wang et al. [16]	This work
V_{IN}	100 mV	1 V	250 mV	185 mV
E_{OUT}	470 μJ	480 μJ	1.02 mJ	1.1 mJ
Efficiency	68%	35%	25%	42%
V_{OUT}	1.8–5.5 V	3.3 V	3.3 V	3.3 V

the EH, in the charge regime. At the initial charge, the LDO output presents a low efficiency. This is mainly because of the low voltage state (2.3 V) that the AUX capacitor has at that time, and the internal efficiency of the LDO embedded in the IC. But, in contrast, the OUT output presents a higher efficiency compared to LDO, ranging from 40% to 51%. To understand the relevance of this information, a comparison was made with other studies (Table 4).

In comparison with other proposals, the current EH configuration provides a higher energy output than the rest. In efficiency, Desai et al. [30] proposal has the highest value but is closely followed by this work.

With this information, it is possible to estimate the time that the energy harvester will take to charge the energy reservoirs of the load, at least in the initial phase when these do not present any charge. To minimize the amount of time the reservoirs take to charge, it is important that the load remains inactive until the stable regime has been achieved.

Having stated that the behaviour of the LTC3108 varies according to the different work regimes, the analysis of the stable regime was done and presented in Figure 10.

In Figure 10, it is possible to see that there are two charge scenarios for the LDO output in this regime. The first scenario is when the output capacitor of OUT is fully charged to its nominal value (3.3 V), and the AUX capacitor has a lower or the same value. In this case, the LDO is charged at the same rate as the OUT capacitor would be charged, thus presenting a higher efficiency. The second scenario is when the AUX capacitor is charged at a higher voltage than the OUT output capacitor, up to 5.2 V. In this case, the efficiency is lower than in the first scenario due to the internal composition of the IC, which limits the amount of current drained to the LDO capacitor [24]. In both regimes, the OUT efficiency remains the same.

In average, the amount of energy that can be extracted in the stable regime from the LDO output is 519 μJ, in its worst charge scenario ($V_{AUX} > V_{OUT}$), and from the OUT output 1.1 mJ. Knowing this, it is possible to state that more than enough energy is generated to maintain both the MCU and transceiver in their inactive states and sparingly charge the energy reservoirs for the active states, according to Table 1.

As mentioned before, these analyses were done without the use of a storage device, which would help increase the charge rate of the output capacitors. Nonetheless, this scenario was also tested, and with a charged supercapacitor of 470 mF it was able to provide an average of 5 mA of current, charging the output capacitors at a very high rate.

Knowing the amount of energy required by the load (Table 2), and realizing that the energy provided by the EH block will not suffice to supply the load in active state by its own, the next step was to estimate the size of the energy reservoirs that would supply the active pulse consumption. For the energy reservoirs, supercapacitors were selected due to their high density and excellent performance under pulse load conditions. To calculate the minimum capacity required, the following formula was employed:

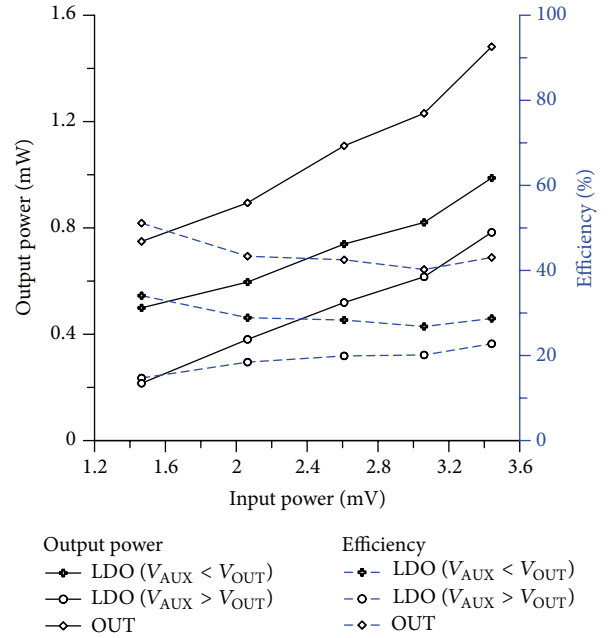

Figure 10: Power and efficiency comparison in stable regime. The obtained power is shown with continuous lines and the efficiency with dashed lines.

$$C = \frac{2\varepsilon}{V_2^2 - V_1^2}. \quad (2)$$

Formula (2) shows the capacity of the energy reservoirs for the LDO and OUT outputs, where C is the capacitance in farad, ε is the energy in joule, V_1 is the lowest voltage supported, and V_2 is the nominal voltage. Depending on whether the calculations are done for the MCU or the transceiver, the voltages will vary according to their individual supply and limitations (Table 5).

Having calculated the size of the supercapacitors, it is also important to consider the peak current that will be demanded by the load, as this will define the minimum ESR of the supercapacitors. According to their corresponding datasheets, the MCU consumes a maximum of 24 mA and the transceiver at least 154 mA while transmitting. With this

Table 5: Supercapacitor calculations for the load, according to the active energy consumption per scenario.

One-hour cycle					
Measurements	Transmissions	MCU		Transmitter	
(per cycle)	(per cycle)	Active energy (mJ)	Capacitance (mF)	Active energy (mJ)	Capacitance (mF)
360	1	122.6	291.9	240.2	133.4
60	1	78.72	187.4	240.2	133.4
6	1	70.82	168.6	240.2	133.4
1	1	70.08	166.9	240.2	133.4

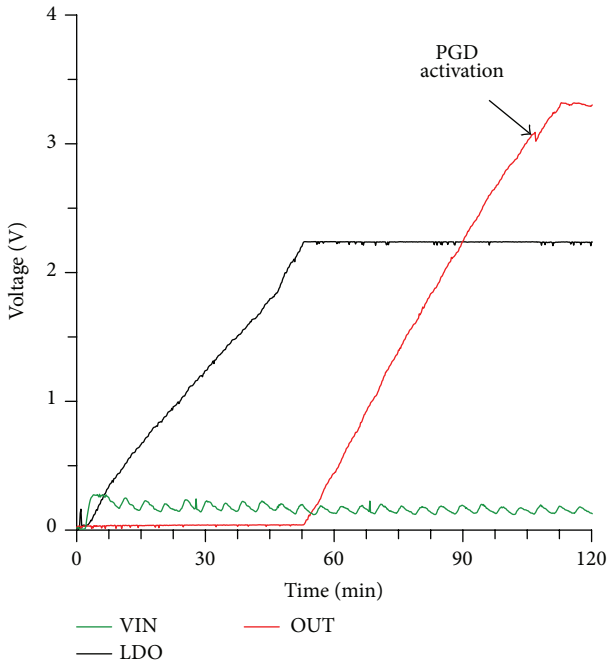

Figure 11: Charge time for the output supercapacitor versus harvested energy, at start-up.

in mind, and using the transceivers current as reference, the supercapacitors will require having an ESR lower than 20 Ω.

Afterwards, a time-based analysis was done in conjunction with the energy harvesting module. This will allow for a validation of the start-up time required by the mote. For this test, one of the previously mentioned operation cycles has to be selected; thus, the scenario with 60 sense measurements per hour was chosen, as it represents a middle point between all the cycles. As the values of capacitance in Table 5 are nonstandard, 2 × 100 mF supercapacitors were chosen for the MCU and transceiver each. Next, the TEG was connected to the EH module, the supercapacitors were placed on each output, and voltage on each output, as well as at the EH input, was measured every 10 seconds (Figure 11).

As seen in Figure 11, the initial start-up takes approximately 100 minutes to charge up to the point that the PGD signal is activated, thus connecting the load to its supply voltage and initializing its work cycle. This scenario may seem unfavourable for the sensor, due to the loss of data for the first 100 minutes, but the reality is that this charge behaviour would only happen on its first usage or after it has not been utilized for a long period of time and the supercapacitors have been fully discharged. Also, this initial charge time may vary depending on the amount of energy generated by the EH block at the time; thus, having more energy will decrease the charge time of the supercapacitors.

With the previous data, it is clear that increasing the amount of sensor measurements may impact greatly the initial start-up, as it would require bigger supercapacitors. Thus, the previously selected operation cycle of 60 measurements and 1 transmission will be used as a basis for the next tests.

Having validated each block of the mote individually, in the next section, the verification of all working parts as a whole will be described.

4.5. Mote Validation. With the data extracted from the previous analyses, the next step was to validate the mote (Figure 12) as a whole by testing it in an actual home environment for a 24-hour time span.

There are two main scenarios that must be distinguished in this test, an 8-hour active period and a 16-hour inactive period. The active period represents the 2PM to 10PM time span, and the inactive period characterizes the span where the heat radiator is shut down. Analysing the inactive period will allow for an understanding of the supercapacitor discharge and the amount of energy required for a system reboot at the following day of operation. The 2–10PM time span was chosen because it is a usual operating cycle of a CH system.

For this test, a 470 mF supercapacitor was used for the STORE output, as well as the 2 × 100 mF for the LDO and OUT outputs each. Voltage measurements were done at the EH input, STORE, LDO, and OUT outputs every 10 seconds. To verify the successful data transmission to the WiFi server, the Wireshark [32] software was utilized (Figure 13).

The first thing to notice in Figure 13 is the OUT and LDO output transmission energy consumption spikes, which decrease with each transmission. This behaviour is due to the energy that is being accumulated in the STORE supercapacitor, which allows for a faster recharge between transmissions.

Due to the initial start-up time, only 6 transmissions were able to be sent to the WiFi server. The success rate of these transmissions was 100% according to the data captured with Wireshark.

As an additional test, the same voltage measurements were done for an extended period of time, until the mote sends an additional transmission. This test emulates the behaviour of the mote and supercapacitors on a continuous work cycle (Figure 14).

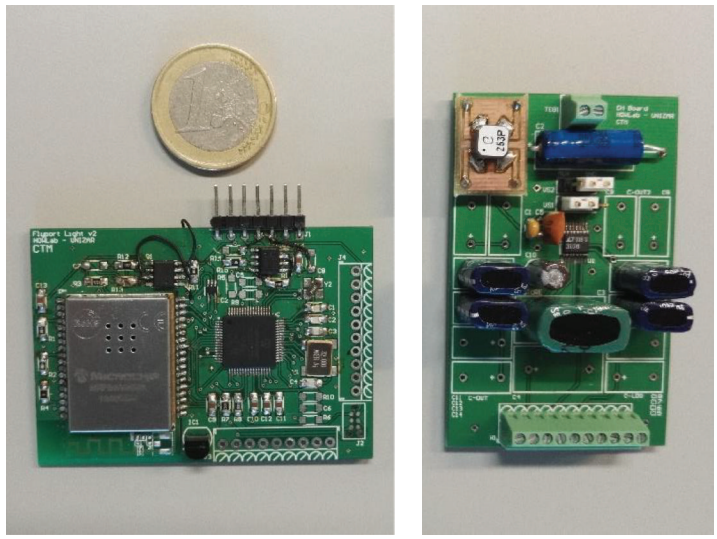

(a) (b)

Figure 12: Prototype boards of the mote, with the load (a) and EH block (b). Both boards are missing some components as they are for future usage.

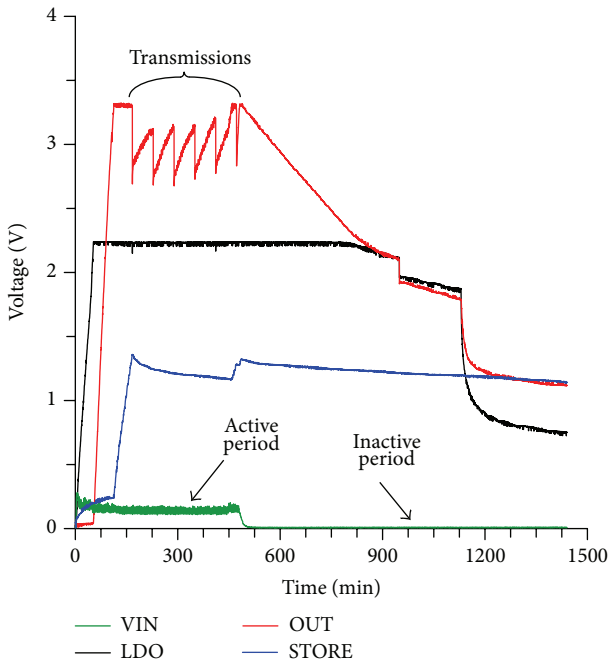

Figure 13: 24-hour actual home scenario test of the mote.

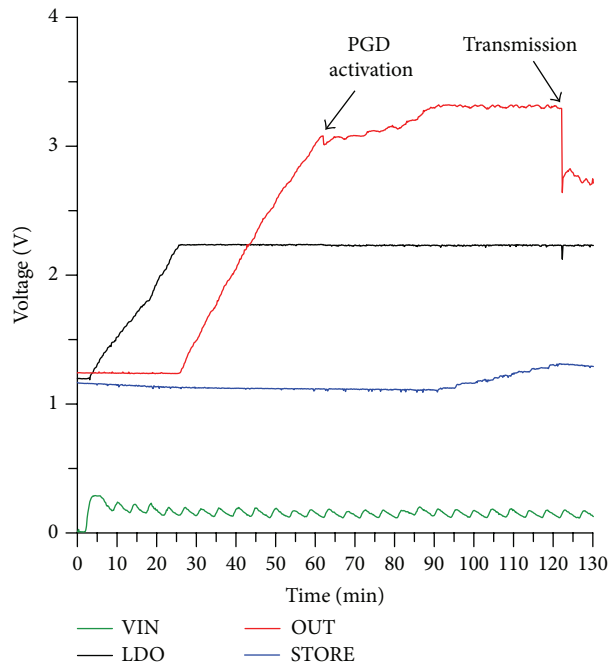

Figure 14: Extended actual home scenario reboot test of the mote.

With this test, it is possible to see the faster reboot of the mote back to operation (approximately 40 min.), compared to the initial start-up. This increase in charge time allows for more energy to be accumulated in the STORE supercapacitor that can be used to recharge the other outputs faster and reserve more energy for the next day of operation. Potentially, this extra energy reserve will allow for an even faster reboot on the next day of operation. Also, having a faster reboot grants more transmissions than at the initial start-up.

4.6. Mote Sustainability. Sustainability can be defined as the capacity of a system, device, or application to endure for a given time period, whether it is definite or indefinite. In applications such as the current proposal, sustainability can be divided into two areas, operating and energy. These will constrain the application under a specific operating window. Under a given operating cycle time frame, the energy sustainability is determined by two factors: the amount of energy generated at the outputs by the EH block and

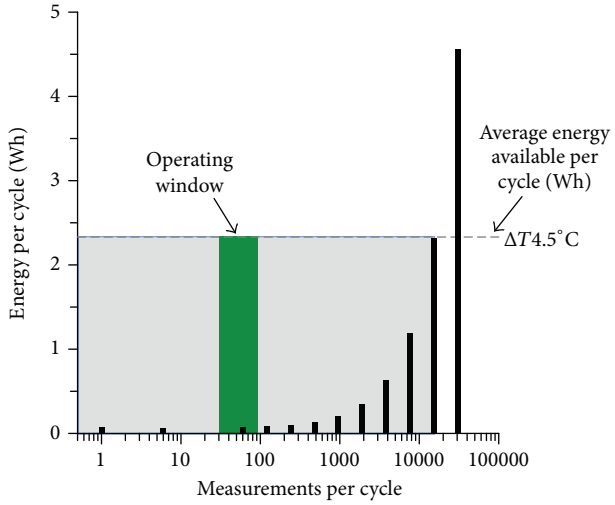

Figure 15: Energy and operating sustainability graph of the mote for different measurement scenarios. The grey area depicts the maximum amount of measurements with the average energy. For this study, a cycle is considered to be 1 hour.

the energy consumed by each activity of the load, as well as their energy consumed while being inactive. On the other hand, the operating sustainability is defined by the minimum amount of temperature measurements that will provide valid information to the user and the maximum amount of measurements that can be done with the useful energy stored in the supercapacitors of the MCU.

As stated previously, the initial setup condition of the mote is an operation cycle time frame of 1 hour, where a single data transmission is done. Given the characteristics of the energy management IC, output capacitors for the MCU and transceiver of 200 mF each were selected. This provides enough energy for each activity and an adequate start-up time. Given these conditions, a sustainability analysis was done to find the proposed operating window which will define the best application scenarios for this proposal. It is important to note that this analysis only considers the stable regime, as in the charge regime there are no activities done (Figure 15).

In Figure 15, based on the experimental measurements (Table 1), calculations were made to obtain the amount of energy consumed by a wide number of samples in a single cycle and a single transmission. Additionally, the average amount of energy available at the LDO output, at a 4.5°C temperature difference in the specified time cycle, was extracted.

In Figure 15, two main areas can be depicted, one gray colored and another green colored, all being referenced to the 4.5°C average energy level. The grey section symbolizes the maximum amount of measurements that could be done with the average energy available in one hour. Yet, given the constraint of the supercapacitor size, not all of the energy will be used for this purpose, but instead, it will remain stored as backup in an energy reservoir at the STORE output. Having said that there is a limit set by the supercapacitor size, given our initial conditions, the green area comes into place, depicting the optimum operating window of scenarios for the current proposal. The minimum limit set for the green area was defined by the amount of samples required to provide useful information to the user. With a minimum of thirty samples per cycle, it is possible to provide a good sense, albeit a bit rough, of the temperature variations measured, although more samples are recommended.

5. Discussion

As described earlier, one of the key differentiators of this proposal is the integration of WiFi communications with energy harvesting on a sensor mote. Yet, the described device presents similarities with other proposals.

The TEG and EH blocks can be compared to the one used in the Tyndall ZigBee mote, submitted by Wang et al. [16]. In their work, several proposals and devices were analysed so as to select the best approach for their implementation. Specifically, a comparison is made with the LTC3108 IC, device used in the current work, but only with a 1 : 100 turn ratio transformer which, as also demonstrated here, presents a low efficiency at its main OUT output. However, when analysing this output with a 1 : 50 turn at 3.3 V, the same voltage used in their mote, it has been demonstrated that it is possible to have an efficiency of up to 51%, compared to the 25.2% achieved by their EH block. At the minimum, in this work, an efficiency of 40% is accomplished. If this EH block were to be used with the Tyndall ZigBee mote, only 2.6 mW would be required to be generated by the TEG, as the EH block would generate 1.1 mW at the 3.3 V output. This represents almost a 50% reduction in energy extracted from the ambient. Additionally, the use of a device such as the energy management IC brings the added benefit of having a general purpose EH block, which may be used for harvesting other types of ambient energies.

If ZigBee communications were to be used, instead of WiFi for this implementation, lower start-up times and energy levels could be achieved, decreasing the size of the required supercapacitors. Yet, as previously stated, it would still require the placement of ZigBee specific infrastructure and an additional device which would upload data to the cloud, such as the work of Kelly et al. [18] or Nugroho and Sahroni [20]. This would represent an added economic cost and, because of its uncommon use by the general population, a less user-friendly setup. The advantage that WiFi presents against other protocols such as ZigBee is that having a network infrastructure already in place, as in the majority of households, this can decrease the economic cost of a project and simplify its implementation, as well as the interaction with users.

Another similar approach is the one presented by Nguyen and Le-trung [19]. In their proposal, they also use low power hardware and software techniques with WiFi communications for sensing data in smart buildings, using the same MRF24 transceiver as the one proposed here, and a PIC18 MCU. Yet, they present similar energy consumption, even though in this proposal a PIC24 MCU is used. One of the main reasons for this is that in this work the supply voltage of the MCU was lowered from 3.3 V to 2.2 V, which inherently

lowers its consumption. Also, the use of a cold start-up with the internal LPRC oscillator helped improve the energy demand. Moreover, in this work, sensor measurements can be done every minute, although the transmissions are by default set to run every hour. Another key difference is that for their implementation they use batteries (4×4200 mAh@3.7 V) to achieve a maximum operation of 46 days, whilst in this proposal EH is used which could potentially have no limit of operation. In order to compare both architectures, if we would power our mote with this pack of batteries, we would have 71 days of lifetime.

Seeing that there was enough energy generation to store a part of it (Figure 13), several possibilities are opened. If enough energy is generated by the TEG, it may be possible to increase either the amount of sensor measurements or the transmission rate, creating a more adaptable mote to different operation cycles. Also, the size of the STORE supercapacitor could be increased, which would additionally help in a faster reboot time on each sequential work cycle.

In the 24+ hours' mote tests, it was proven that the implementation is a viable solution to the current problematic. Ideally, it would be desirable to start sensing data as soon as the LDO output has reached its nominal 2.2 V, as this would enable the MCU which manages the temperature sensor. Currently, this is addressed with a faster reboot time with the energy stored after the 8-hour active period; yet, in the first few days of operation, there is some data loss. A possible improvement would be to add an additional start-up circuit that analyses the LDO output directly. This would leave the PGD pin free to be analysed by the MCU, giving it knowledge of the energy availability for the transceiver.

Further analysing Figure 15, with a lower energy availability than the one provided by a 4.5°C temperature difference, it could be possible to work under these same operating windows. Yet, with such an energy output, the initial start-up time for the mote would be increased. On the other hand, having a higher energy availability would grant a quicker initial start-up time and more energy to store for backup. Also, it could be possible to increase the supercapacitors size, accommodating more measurements per cycle or even more transmissions.

A probable improvement to the presented proposal would be the replacement of the MCU, which has a high energy consumption in general. If a PIC24FJ128GA306 [33] MCU from the nanoWatt XLP family were to be selected, a notorious increase in performance could be achieved. This MCU presents a low deep sleep consumption of 10 nA, which consequently would allow for more energy to be stored at a faster rate. Also, its active state current consumption presents a lower value of 6.5 mA, decreasing the minimum size of the LDO supercapacitor to 58 mF. This would represent a reduction in capacity of almost 70%. Assuming the use of the same supercapacitors that are currently set, only 100 mF would be more than enough to cover its demand, decreasing greatly the start-up time. Also, the integration of an energy-aware firmware, as well as the selection of a MCU with a wider supply voltage range, would allow for decisions over each activity to be taken by the mote and a reduction in size of the output supercapacitors.

On the transceiver side, the transmission output power could be modulated according to the needed signal strength required to communicate with the access point. In the majority of home scenarios, it is possible that a 10 dbm output is not required, and decreasing it would improve the consumption greatly. Moreover, depending on the scenario, the UDP protocol could be used to decrease the transmission time and energy consumption, although data delivery would not be assured.

6. Conclusions

In this paper, an autonomous WiFi sensor for auditing home heating devices was presented. A complete analysis of the load was done, giving a clear understanding of the energy needs required. Also, theoretical calculations were made for the needed energy reservoirs, or supercapacitors, and the experimental validation of these was proven. Afterwards, a characterization of the TEG was accomplished, which allowed for the appropriate selection of components for the EH block. With the proper components, the efficiency and power capabilities of the EH block were demonstrated, achieving an increase in performance of 50% compared to other implementations. Finally, all blocks were put to the test as a whole in a practical scenario for 24+ hours, proving the motes' proper functionality in smart home environments.

To conclude, the use of autonomous WiFi sensors as a WSN solution in IoT not only is viable, but also simplifies its implementation thanks to its already widespread network and ubiquity in IoT devices. There are a wide variety of scenarios where WiFi sensors can be implemented to transfer environmental data to the cloud, without the need of additional network communications. Furthermore, it can be easily paired with EH technologies to cover its energy consumption or help recharge its primary battery system for an extended life span.

Conflict of Interests

The authors declare that there is no conflict of interests regarding the publication of this paper.

Acknowledgments

Trasviña-Moreno would like to thank the Consejo Nacional de Ciencia y Tecnología of México for providing the scholarship for his Ph.D. Also, the authors would like to thank the Ministerio de Economía y Competitividad of Spain for Project Memory Lane (MeLa) which this proposal is a part of.

References

[1] Instituto Nacional de Estadística (INE), "Censos de Población y Viviendas 2011 Datos detallados Principales resultados Principales indicadores Tamaño del hogar," 2011.

[2] M. Zago, A. Casalegno, R. Marchesi, and F. Rinaldi, "Efficiency analysis of independent and centralized heating systems for

residential buildings in Northern Italy," *Energies*, vol. 4, no. 11, pp. 2115–2131, 2011.

[3] O. Guerra Santin, "Behavioural patterns and user profiles related to energy consumption for heating," *Energy and Buildings*, vol. 43, no. 10, pp. 2662–2672, 2011.

[4] El Parlamento Europeo y el Consejo de la Unión Europea, *Directiva 2012/27/UE del Parlamento Europeo y del Consejo de 25 de Octubre de 2012 Relativa a la Eficiencia Energética*, Diario Oficial de la Unión Europea, 2012.

[5] IEEE, "IEEE standard for local and metropolitan area networks—part 15.4: low-rate wireless personal area networks (LR-WPANs)," IEEE Standard 802.15.4-2011, 2011.

[6] IEEE Standards, "Telecommunications and information exchange between systems local and metropolitan area networks—specific requirements Part 11: wireless LAN Medium Access Control (MAC) and Physical Layer (PHY) specification," IEEE 802.11, 2012.

[7] D. Niyato, L. Xiao, and P. Wang, "Machine-to-machine communications for home energy management system in smart grid," *IEEE Communications Magazine*, vol. 49, no. 4, pp. 53–59, 2011.

[8] K. Malhi, S. C. Mukhopadhyay, J. Schnepper, M. Haefke, and H. Ewald, "A zigbee-based wearable physiological parameters monitoring system," *IEEE Sensors Journal*, vol. 12, no. 3, pp. 423–430, 2012.

[9] Y. Yan, Y. Qian, H. Sharif, and D. Tipper, "A survey on smart grid communication infrastructures: motivations, requirements and challenges," *IEEE Communications Surveys and Tutorials*, vol. 15, no. 1, pp. 5–20, 2013.

[10] H. Abdelnasser, M. Youssef, and K. A. Harras, "WiGest: a ubiquitous WiFi-based gesture recognition system," in *Proceedings of the IEEE Conference on Computer Communications (INFOCOM '15)*, pp. 1472–1480, Hong Kong, April 2015.

[11] S. Tozlu, "Feasibility of Wi-Fi enabled sensors for Internet of Things," in *Proceedings of the 7th International Wireless Communications and Mobile Computing Conference (IWCMC '11)*, pp. 291–296, IEEE, Istanbul, Turkey, July 2011.

[12] L. Sun, S. Sen, D. Koutsonikolas, and K. Kim, "WiDraw: enabling hands-free drawing in the air on commodity WiFi devices," in *Proceedings of the 21st Annual International Conference on Mobile Computing and Networking (MobiCom '15)*, pp. 77–89, Paris, France, September 2015.

[13] A. S. Weddell, M. Magno, G. V. Merrett, D. Brunelli, B. M. Al-Hashimi, and L. Benini, "A survey of multi-source energy harvesting systems," in *Proceedings of the Design, Automation & Test in Europe Conference & Exhibition (DATE '13)*, pp. 905–908, Grenoble, France, March 2013.

[14] M. Piñuela, P. D. Mitcheson, and S. Lucyszyn, "Ambient RF energy harvesting in urban and semi-urban environments," *IEEE Transactions on Microwave Theory and Techniques*, vol. 61, no. 7, pp. 2715–2726, 2013.

[15] J. W. Matiko, N. J. Grabham, S. P. Beeby, and M. J. Tudor, "Review of the application of energy harvesting in buildings," *Measurement Science and Technology*, vol. 25, no. 1, Article ID 012002, 2014.

[16] W. Wang, V. Cionca, N. Wang, M. Hayes, B. O'Flynn, and C. O'Mathuna, "Thermoelectric energy harvesting for building energy management wireless sensor networks," *International Journal of Distributed Sensor Networks*, vol. 2013, Article ID 232438, 14 pages, 2013.

[17] J. Han, C. Choi, W. Park, I. Lee, and S. Kim, "Smart home energy management system including renewable energy based on ZigBee and PLC," *IEEE Transactions on Consumer Electronics*, vol. 60, no. 2, pp. 198–202, 2014.

[18] S. D. T. Kelly, N. K. Suryadevara, and S. C. Mukhopadhyay, "Towards the implementation of IoT for environmental condition monitoring in homes," *IEEE Sensors Journal*, vol. 13, no. 10, pp. 3846–3853, 2013.

[19] M. Nguyen and Q. Le-trung, "Low-power and cost-effective wifi sensor motes for wireless embedded internet applications," in *Proceedings of the International Conference on Advanced Technologies for Communications (ATC '14)*, pp. 441–445, Hanoi, Vietnam, October 2014.

[20] E. Nugroho and A. Sahroni, "ZigBee and wifi network interface on Wireless Sensor Networks," in *Proceedings of the Makassar International Conference on Electrical Engineering and Informatics (MICEEI '14)*, pp. 54–58, Makassar, Indonesia, November 2014.

[21] Flyport WiFi b—OpenPicus Wiki, September 2015, http://wiki.openpicus.com/index.php/Flyport_WiFi_b.

[22] PIC24FJ256GA106—16-bit PIC® and dsPIC® Microcontrollers, September 2015, http://www.microchip.com/wwwproducts/Devices.aspx?product=PIC24FJ256GA106.

[23] "MRF24WB0MA—rfPIC," 2015, http://www.microchip.com/wwwproducts/Devices.aspx?product=MRF24WB0MA.

[24] LTC3108—Ultralow Voltage Step-Up Converter and Power Manager—Linear Technology, September 2015, http://www.linear.com/product/LTC3108.

[25] "MSO2000/DPO2000 Mixed Signal Oscilloscopes/Tektronix," 2015, http://www.tek.com/datasheet/mso2000-dpo2000/mso2000b-series-dpo2000b-series-datasheet.

[26] "DMM4050/4040 Digital Multimeter Digital Multimeters Datasheet/Tektronix," 2015, http://www.tek.com/datasheet/dmm4050-4040-digital-multimeter.

[27] "TC-08 Thermocouple data logger/Pico Technology," 2015, https://www.picotech.com/data-logger/tc-08/thermocouple-data-logger.

[28] LabVIEW System Design Software—National Instruments, September 2015, http://www.ni.com/labview/.

[29] C. A. Trasviña-Moreno, A. Asensio, R. Casas, R. Blasco, and A. Marco, "WiFi Sensor Networks: a study of energy consumption," in *Proceedings of the IEEE 11th International Multi-Conference on Systems, Signals & Devices (SSD '14)*, pp. 1–6, IEEE, Barcelona, Spain, February 2014.

[30] N. V. Desai, Y. Ramadass, and A. P. Chandrakasan, "A bipolar ±40 MV self-starting boost converter with transformer reuse for thermoelectric energy harvesting," in *Proceedings of the International Symposium on Low Power Electronics and Design (ISLPED '14)*, vol. 14, pp. 221–226, La Jolla, Calif, USA, August 2014.

[31] H. Lhermet, C. Condemine, M. Plissonnier, R. Salot, P. Audebert, and M. Rosset, "Efficient power management circuit: thermal energy harvesting to above-IC microbattery energy storage," in *Proceedings of the IEEE International Solid-State Circuits Conference (ISSCC '07)*, Digest of Technical Papers, pp. 62–587, San Francisco, Calif, USA, February 2007.

[32] Wireshark, September 2015, https://www.wireshark.org/.

[33] "PIC24FJ128GA306—16-bit PIC® and dsPIC® Microcontrollers," 2015, http://www.microchip.com/wwwproducts/Devices.aspx?product=PIC24FJ128GA306.